



## Direct ink writing techniques for in situ gelation and solidification

**Jackson K. Wilt**, Chemical Sciences Division, Oak Ridge National Laboratory, Oak Ridge, TN 37831, USA

**Dustin Gilmer**, Chemical Sciences Division, Oak Ridge National Laboratory, Oak Ridge, TN 37831, USA; The Bredesen Center for Interdisciplinary Research and Graduate Education, The University of Tennessee, Knoxville, TN 37996, USA

**Sungjin Kim**, Chemical Sciences Division, Oak Ridge National Laboratory, Oak Ridge, TN 37831, USA

**Brett G. Compton**, Department of Mechanical, Aerospace, and Biomedical Engineering, The University of Tennessee, Knoxville, TN 37996, USA

**Tomonori Saito**, Chemical Sciences Division, Oak Ridge National Laboratory, Oak Ridge, TN 37831, USA; The Bredesen Center for Interdisciplinary Research and Graduate Education, The University of Tennessee, Knoxville, TN 37996, USA

Address all correspondence to Tomonori Saito at [saitot@ornl.gov](mailto:saitot@ornl.gov)

(Received 23 September 2020; accepted 9 December 2020; published online 24 February 2021)

### Abstract

Direct ink writing (DIW) is an extrusion-based 3D printing method which prints near ambient temperatures and has one of the broadest printable material selections among additive manufacturing techniques. However, DIW uses viscoelastic materials susceptible to collapse during printing. One promising route to improve the structural integrity of viscoelastic inks is using in situ curing methods to increase the yield strength of the printed structures after deposition. This review summarizes progress in three representative methods of in situ curing for DIW, including ultra-violet-induced crosslinking, rapid cure of reactive ingredients, and flash vaporization of a solution's solvent to coagulate dissolved polymers.

**Keywords** 3D printing · In situ · Direct ink writing · Photochemical · Solvent casting

### Introduction

Additive manufacturing (AM), commonly referred to as three-dimensional (3D) printing, produces 3D components layer-by-layer, using digital designs. While there are many AM methods, stereolithography (SLA), digital light processing (DLP), and fused filament fabrication (FFF) are the most well-known AM methods, partly due to the extended history of their development.<sup>[1]</sup> However, these methods still have challenges such as limited materials selection for SLA and DLP as well as weak interlayer bonding and residual stresses in FFF. SLA and DLP are two popular AM methods that use ultra-violet (UV) light to solidify/cure photopolymerizable masks of low viscosity resin.<sup>[2]</sup> These light-based lithography methods use mixtures of (often proprietary) photocurable resins and optically transparent fillers, limiting high additive loading and complex materials formulations.<sup>[3,4]</sup> One popular methodological approach to avoid some of the limitations of UV AM is to utilize a material extrusion process, in which a nozzle selectively deposits material according to a digitized print path. One of the most prevalent material extrusion methods in industry and research fields is FFF, which uses thermoplastic material extruded from a heated nozzle.<sup>[5]</sup> However, the FFF method is limited to thermoplastic materials and has challenges with residual stresses imparted by thermal gradients during the printing process as well as interlayer weakness.<sup>[6]</sup> These limitations of FFF have incentivized advancements in ambient temperature extrusion

with features of interlayer crosslinking to improve isotropic properties.

Direct ink writing (DIW) is an extrusion-based AM method that uses viscoelastic inks deposited typically at or slightly above room temperature to realize 3D objects.<sup>[7,8]</sup> In principle, DIW represents the combined advantages of FFF, SLA, and DLP. DIW exploits material extrusion-based methods similar to FFF, utilizes a broad array of materials systems, and is capable of multi-material printing. DIW also takes advantage of ambient temperature operation with curable resin-based materials similar to SLA and DLP. Many DIW ink resins are thermosets designed to crosslink upon curing to form high-strength solids. Thermosets are used because the thermoset resins provide a viscous base that can easily be mixed with additives to create printable inks. In addition, the crosslinked structure of the thermosets in DIW provides interlayer strength as strong as a cast component, compared to weak interlayer strengths in FFF components.<sup>[6]</sup> Aside from material systems mentioned previously, soft materials such as silicones,<sup>[9]</sup> epoxy,<sup>[10]</sup> hydrogel,<sup>[11]</sup> and preceramic polymer,<sup>[12,13]</sup> along with composite additives such as carbon nanotubes,<sup>[14]</sup> carbon fiber,<sup>[15]</sup> graphene,<sup>[16]</sup> liquid metals,<sup>[17]</sup> and other ceramics<sup>[18,19]</sup> are material systems largely exclusive to DIW.

Despite all of the positive aspects of using viscoelastic thermosetting materials in DIW, they retain fluid-like properties until sufficiently cured through crosslinking or solidification

and pose the risk of collapse under self-weight stress.<sup>[20]</sup> Once the stress from the weight of uncured print layers exceeds the ink's internal yield strength, the lower layers begin to yield. In some cases, the inks shear perpendicular to the building height or experience buckle-induced failure of the uncured structure.<sup>[21]</sup> Print collapse occurs even more prevalently during post-process thermal curing, which is common for DIW, due to the reduced viscosity of the inks and lower yield strengths at elevated temperatures before crosslinking. In contrast, FFF does not encounter yielding issues during printing because thermoplastic material solidifies shortly (several seconds) after deposition. In DIW, however, the viscoelastic yield strength and thixotropic recovery of the materials are insufficient to create extensive self-supporting architectures. Thixotropy is a time-dependent recovery behavior found in viscoelastic materials. For some DIW instances, the viscoelastic inks do not have adequate time to recover after the deposition process to withstand the weight of subsequent layers. This issue calls for methodologies to significantly increase the yield strength of DIW inks while printing. If the yield strength can be improved and controlled during the DIW process, the applications of DIW will expand vastly and provide geometrically complex objects compared to FFF while having customizable materials systems. Due to the easily tailorable materials systems, DIW-printed components can exhibit greater mechanical and functional properties compared to components in other AM methods.<sup>[7]</sup>

This review focuses on advancements in DIW processes to address the challenge of preserving and enhancing yield strength for self-supporting structures while printing. These process advancements include the use of external-stimuli-induced polymerization, rapidly curing thermosets at ambient temperatures, and molecular agglomeration through solvent evaporation to increase the yield properties while printing (Fig. 1).<sup>[22, 23]</sup> The review will start with the fundamental requirements for DIW inks, followed by three main process advancements in DIW: (1) DIW UV-assisted cure (UVA-DIW), where material extrusion is followed by UV-curing exposure, (2) reactive additive manufacturing (RAM), which uses rapid polymerization to form thermosets through exothermic crosslinking at ambient temperatures, and (3) solvent cast 3D printing (SC-3D), where particulates or other polymers are coagulated upon the evaporation of solvent from the ink at atmospheric pressure. These in situ processing techniques improve two main engineering shortcomings of DIW. First, in situ curing enhances the geometric capabilities of DIW by improving achievable span lengths and high-angle overhangs. Conventional DIW geometric capabilities are dependent on additive loading and thixotropic recovery of the ink, but with in situ curing solidification, the constraints on minimum filler loading are alleviated.<sup>[24]</sup> Second, utilizing in situ polymerization on the print bed allows for parts to retain shape during thermal post-processing, such as polymerization or imidization, because of partial intermolecular-crosslinking. Both of these engineering improvements are critical for more widespread adoption of in situ DIW by

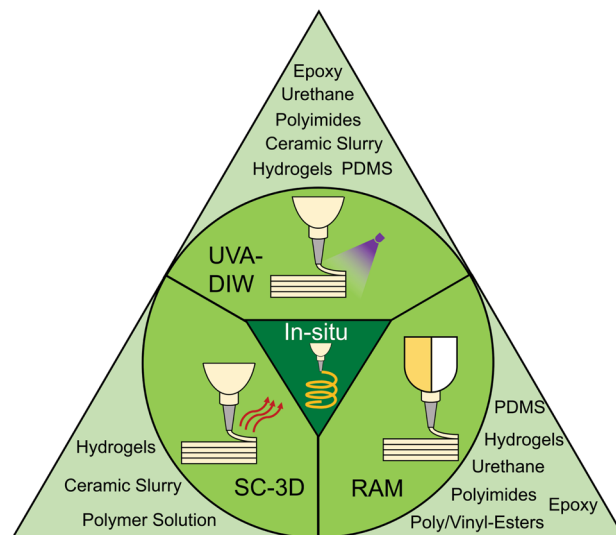


**Figure 1.** Schematic depiction of material-method categories of DIW in situ curing.

offering comparable print geometries to other AM methods, while providing broad options for selection of materials for future applications.

## Properties of DIW inks

DIW inks are viscoelastic materials, whose dynamic mechanics depend on shear rate and shear stress, exhibiting shear-thinning and thixotropic properties. Current DIW also requires extrudable, self-supporting, and shrink-resistant inks governed by their materials' constituents and chemistry. Analytical non-Newtonian fluid models, such as the Herschel–Bulkley (Fig. 2a), can describe the flow of inks and the change in viscosity as it exits the nozzle due to shear-based stimuli and how the structure yields under self-weight after being deposited. The Herschel–Bulkley model contains material flow parameters defined as flow index ( $n$ ) and consistency index ( $K$ ), with the imparted shear rate ( $\dot{\gamma}$ ), to describe the shear-rate-based shear stress. The internal shear stress ( $\tau$ ) is the addition of yield stress at zero shear rate ( $\tau_y$ ) and the shear-rate-based shear stress ( $K\dot{\gamma}$ ). The yield strength of the material coincides with the self-weight-induced shear stress that uncured structures can endure before becoming unstable. The viscosity of DIW printable inks lowers at higher shear rates in accordance with these fluid models, allowing for extrusion and a uniform flow velocity near the center of the nozzle and a pronounced velocity decrease near the nozzle walls.<sup>[23, 25, 26]</sup> The structural integrity of the uncured ink upon deposition is related to the rheological properties, including the viscosity ( $\mu$ ), yield strength ( $\tau_y$ ), and loss factor (i.e., the ratio between the loss and storage modulus,  $\tan\delta = G''/G'$ ) at printing shear rates.<sup>[26, 27]</sup> One of the primary methods to tailor the rheological properties, and thus printability, is by optimizing the volumetric percentage of the matrix polymer, diluent (solvent), and filler (solids with varying size and morphology).<sup>[25, 28–30]</sup> The volumetric percent of filler

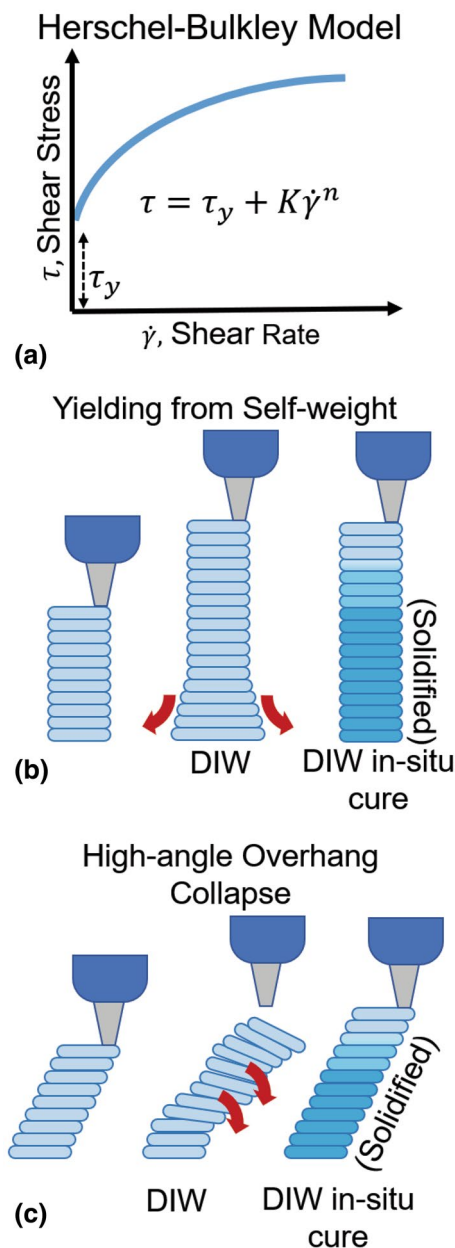


**Figure 2.** Flow behavior and viscoelastic failure modes. (a) Herschel–Bulkley model describing viscoelastic behavior. (b) Yielding of viscoelastic structure from self-weight. (c) High-angle overhang collapse of viscoelastic material.

material, ( $\varphi$ ), is one of the common viscosity-defining parameters studied for producing printable and self-stabilizing inks.<sup>[31, 32]</sup> The approximate range of printable viscoelastic properties at printing shear rates are reported as follows<sup>[27]</sup>:

$$\begin{aligned} \tau_y &> 10^3 \text{ Pa,} \\ \mu &= 0.1\text{--}10^3 \text{ Pa/s,} \\ \tan \delta &< 0.8\text{--}1. \end{aligned}$$

Inks also exhibit a thixotropic behavior, where the inks lower in their yield strength directly after exiting the print nozzle and tend to recover to their unsheared properties over a short duration. Hydrogen bonds or other weak intermolecular interactions contribute to the yield strength of the material prior to and after extrusion. However, a potential issue of the inks includes bond breakage after agitation or during extrusion of the ink through the nozzle resulting in lower viscosity and yield strength. The decrease in viscosity and yield strength after extrusion/deposition causes a period of structural instability that could induce print collapse before the unsheared properties recover. In order to improve the viscoelastic structural properties of printed inks, in situ curing is used to partially or fully cure the structure while printing to enhance the yield strength. The yielding failure mode occurs from the weight of the structure surpassing the yield strength of the lowest layers causing deformation of the base layer out from underneath the structure (Fig. 2b). Overhang collapse is also common when printing overarching layers without underlying support structures (Fig. 2c). Progressive in situ curing makes the yield strength less dependent on the passive viscoelastic structural properties and more reliant on the rate of solidification after deposition, allowing for a broader selection of ink formulations that avoid these failure modes.

### UVA-DIW

UVA-DIW uses UV light to selectively crosslink photocurable monomers within DIW inks while printing. UVA-DIW uses a conventional 3-axis electromechanical stage, common for extrusion-based 3D printers with an additional powered UV light source on or near the point of extrusion. The light sources are typically an array of light-emitting diodes for ambient curing of the entire structure or a penlight that directs the UV light to individual filament sections. These systems have average wavelengths 300–400 nm, and variable power settings govern the energy input from the light source.

The degree of UV solidification is determined by the amount of photo-crosslinkable building blocks in the ink formulation. However, UV light penetration can be impeded when formulations contain high refractive index filler materials, which are common in DIW.<sup>[33]</sup> Studies have generally determined that ceramic materials with low refractive indexes  $n < 1.9$ , including  $\text{SiO}_2$ ,  $\text{Al}_2\text{O}_3$ , tricalcium phosphate, and hydroxyapatite are printable with UV-curable methods despite some UV light scattering. However, larger refractive index additives such as  $\text{Y}_2\text{O}_3$ ,  $\text{Si}_3\text{N}_4$ ,  $\text{ZnO}$ ,  $\text{ZrO}_2$ ,  $\text{BaTiO}_3$ ,  $\text{SiC}$ , and  $\text{TiO}_2$  with  $n > 1.9$  considerably inhibit the curing depth of the UV-induced polymerization. It should be noted aside from the type of filler that  $\varphi$  as well as the filament size and UV energy input to the filaments significantly influence the UV-curing rate and the increase of the yield strength.

UV light is a common stimulus in other additive manufacturing frameworks such as SLA and DLP, which provides

similar curing behavior frameworks of photopolymers that are applicable to UVA-DIW.<sup>[34, 35]</sup> The curing framework analytically determines the level of resin polymerization described by curing depth  $C_d$  (Eq. 1), curing width  $C_w$  (Eq. 2), where an  $E$  (exposure parameter) is established using (Eq. 3). The parameters used in these equations (Eqs. 1–3) are  $D_p$  (penetration depth),  $E_c$  (critical exposure to initiate polymerization),  $F$  (laser spot size),  $n$  (refractive index of the material),  $p_0$  (power of the laser at resin surface),  $w_0$  (radius of the laser beam), and  $v_s$  (laser scanning speed).<sup>[36]</sup> This framework is useful for determining the UV printing speed and energy input with respect to the size of the filament by extrapolating these parameters to the respective UVA-DIW hardware and material systems.

$$C_d = D_p \ln \frac{E}{E_c}, \quad (1)$$

$$C_w = F \sqrt{\ln \frac{E}{nE_c}}, \quad (2)$$

$$E = \frac{2p_0}{\pi w_0 v_s}. \quad (3)$$

High-performance polymers such as polyimides typically require multi-step processing due to their high melting temperature and solvent resistance. UVA-DIW with dual-cure crosslinking systems has taken advantage of the multi-step processing required for polyimides. Photosensitive polyimide precursors were printed using UVA-DIW with a dual-cure crosslinking approach, resulting in printed parts with good interlayer strength and reduced shrinkage.<sup>[37, 38]</sup> Dual-cure systems use UV light for curing the photosensitive portion of the ink, then the second phase of full curing occurs at an elevated temperature. In this case, the dual-cure systems focused on extruding polyimide precursors exposed to UV light for the first-stage cure and then thermally imidized to form fully stable polyimides.<sup>[37, 38]</sup>

Guo et al. used UV crosslinking of hydroxyethyl methacrylate (HEMA)-grafted poly(amic acid) (PAA) as the photosensitive ink component (Fig. 3a).<sup>[38]</sup> The molar percent of 30% HEMA was selected because it provided sufficient gelation from the UVA-DIW light source and allowed for a significant percentage of imide in the final component. The photocurable bond formation of HEMA provided mechanical stability before and during the thermal imidization process. A drawback of imidization techniques is shrinkage during the post-process thermal cure. UVA-DIW-printed parts using the PAA-HEMA precursor exhibited a post-print thermal cure dimensional shrinkage of 8% and tensile strength of ~90 MPa.<sup>[38]</sup> FFF processes have also been used to print polyimides with low-dimensional shrinkage. However, they exhibit an anisotropic mechanical behavior because of interlayer weaknesses, whereas parts printed using DIW exhibit improved mechanical isotropy. The benefit of using UVA-DIW HEMA method to produce

polyimides compared to the other techniques is that the HEMA gelation mitigates the shrinking of the final part by creating intermolecular covalent bonds reinforcing the partially cured matrix.

Wu et al. investigated addition-type bismaleimides (BMI), another form of thermoset polyimides with remarkable thermal and structural properties.<sup>[39]</sup> The process combines BMI and ink consisting of a photocurable mixture with 4,4'-bismaleimidodiphenyl, 2,2'-diallylbisphenol A, and Irgacure 819, followed by UV printing to solidify the structure before final thermal imidization (Fig. 3b). The UVA-DIW dual-cured BMI exhibited a shrinkage of 2–3%, Young's modulus of ~4 GPa, and a thermal decomposition temperature of 370°C, which is comparable to cast BMI components. This study also exhibited complete solidification and curing of the photopolymerizable double bonds within the BMI ink. Solidifying the material using the UV light provided greater yield strength and greater storage modulus, which improved the printing of overhang geometries. The maximum overhang angle achieved by this method was 52° with respect to the build plate, which is significant improvement compared to conventional DIW methods.

UVA-DIW has also been utilized to print shape memory elastomers out of photopolymerizable urethane acrylates.<sup>[40]</sup> In this study, UVA-DIW plays a key role in photopolymerizing an elastomeric network that sets a shape memory configuration (Fig. 4a). The UV light curing is confirmed by the reduction of C=C bonds within the material after a photopolymerization phase. This photo-crosslinked acrylate network confines the semi-crystalline thermoplastic poly(caprolactone) chains, preserving the original shape memory configuration. The UVA-DIW shape memory behavior was exhibited by deforming the UV-cured print, followed by recovering the original shape at temperatures above 76°C [i.e., semi-crystalline poly(caprolactone) melting temperature]. In addition to UV providing the shape memory configuration, photopolymerizing the elastomeric network every successive layer resulted in strong interlayer in situ crosslinking.

Aside from shape memory elastomers, there have also been efforts in manufacturing freeform micro-coil sensors using photopolymerizable urethanes.<sup>[41–43]</sup> In one study, a photoinitiated urethane nanocomposite was printed with the UVA-DIW process, using single-walled carbon nanotubes (CNT) as an electrically conductive filler to measure electrical resistance under tension and compression.<sup>[42]</sup> In the study, micro-coils were printed using a urethane ink containing a photoinitiator exposed to two high-intensity UV light-emitting diodes during printing. This urethane nanocomposite formulation utilized a thiol-ene crosslinking reaction through UV-photoinitiated thiyl radicals. The CNTs were functionalized with carboxylic groups to form hydrogen bonds within the prepolymer matrix. Fumed silica nanoparticles were used in the formulation to improve shear-thinning properties, while the hydrogen bonds enhanced the ink's thixotropic behavior. The rapid gelation of thiol-ene reaction provided self-support for the dramatically high overhang angle in freeform manufacturing of micro-coils



**Figure 3.** UVA-DIW imide precursor dual-cure systems. (a) UVA-DIW of PAA-HEMA with photo-cured and imidized stages of the precursor system.<sup>[38]</sup> Copyright 2019 John Wiley and Sons. (b) Polybismaleimide precursor printing process (I) mixing of PAA precursor, (II) UVA-DIW printing (III), thermal imidization heat treatment, and (IV) fully imidized component and chemistry.<sup>[39]</sup> Copyright 2019 Elsevier.

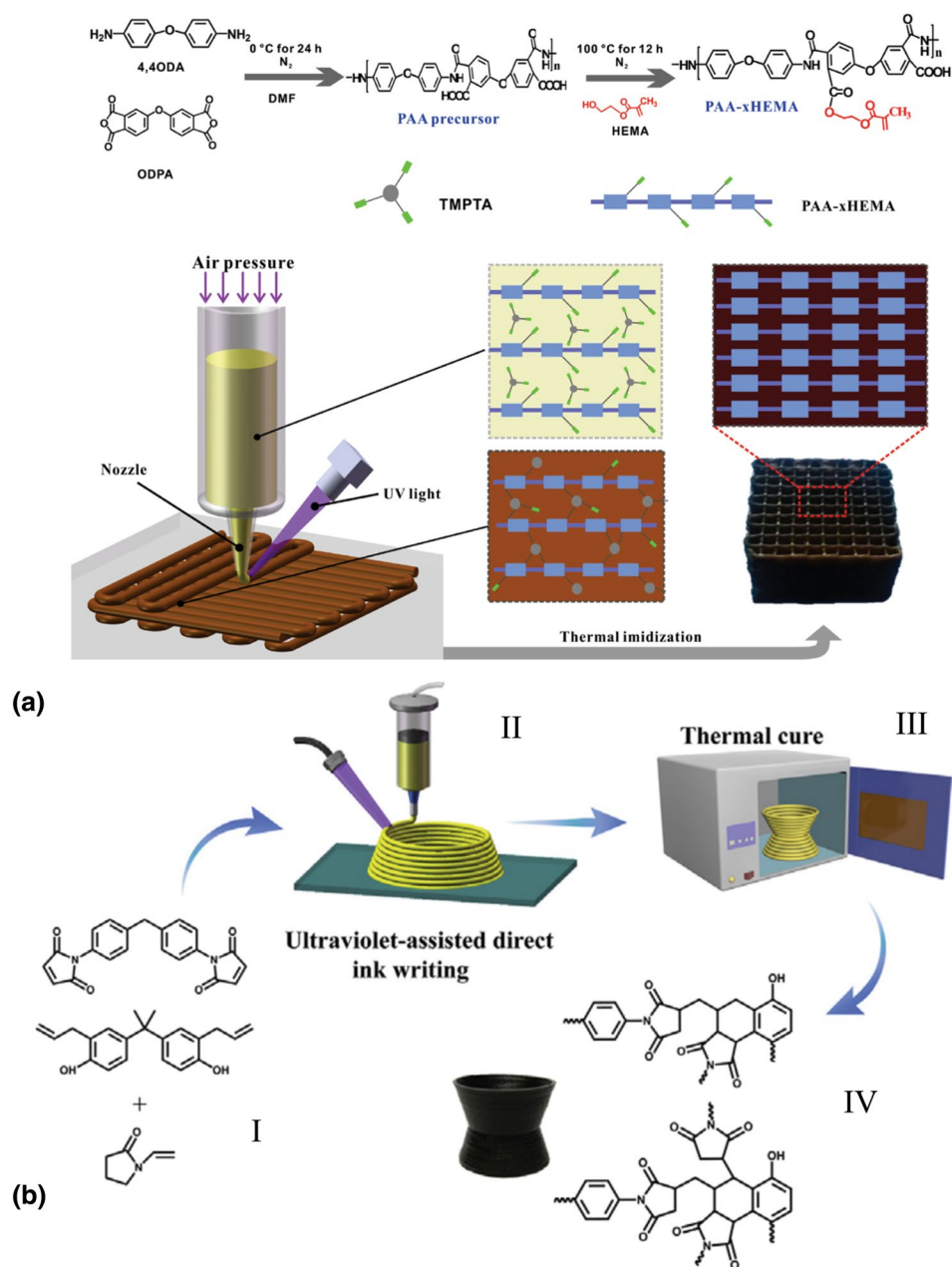


(Fig. 4b). Furthermore, this study contains the transition length of uncured to self-supporting solidification for UVA-DIW, which can be broadly applied to the other UV in situ curing material systems.

Another study investigated shape memory epoxy nanocomposites using a dual-cure system of UVA-DIW.<sup>[44]</sup> This dual-cure system was used to cure a nanocomposite epoxy ink by first performing UV curing of the photocurable acrylates, followed by thermally curing the epoxy. The photosensitive acrylate had an optimal photo-absorption polymerization at 365 nm and subsequent thermal crosslinking pre-cured at 100 °C for 2 h and post-cured at 150 °C for 1 h (Fig. 5a). The UVA-DIW process with the epoxy nanocomposite achieved

the printing of complex objects with large overhangs and high-resolution features (Fig. 5b). Each layer was exposed to the UV light for 10 s, and the amount of time it took for a layer to become fully cured was measured at 70 s total, or seven irradiation steps (Fig. 5c). The elastomeric network exhibited shape memory effects when the material was deformed above its glass transition temperature at 76 °C, cooled below glass transition, and subsequently reheated to return to the printed shape. After being heated back above its glass transition temperature for 18 s, the deformed shape returned to its UV-induced shape memory configuration (Fig. 5d).

UVA-DIW has been implemented with poly(dimethylsiloxane) (PDMS) elastomers as well because

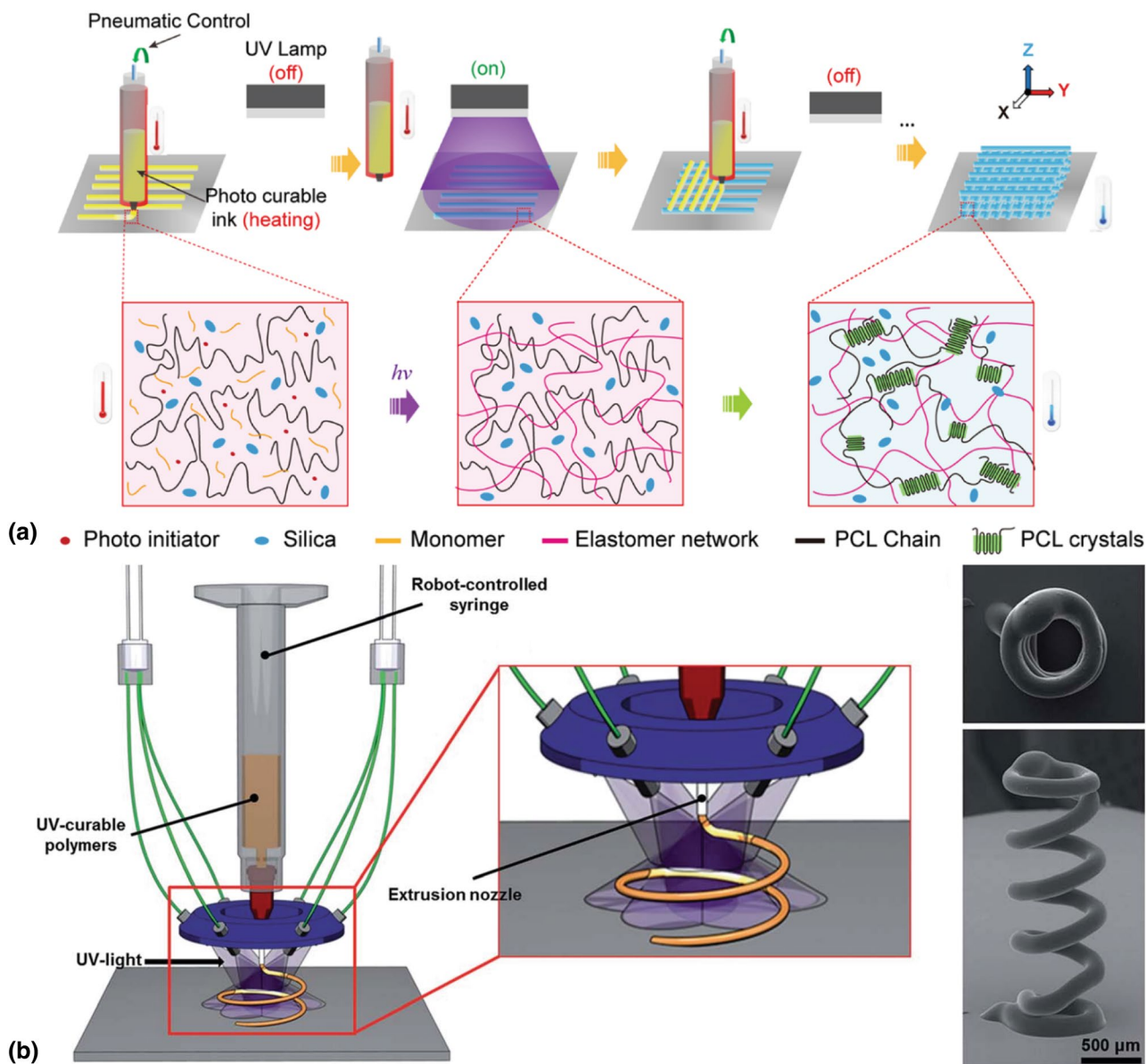


**Figure 4.** UVA-DIW of urethanes. (a) Shape memory urethane printing process.<sup>[40]</sup> Copyright 2018 American Chemical Society. (b) (Left) computer-aided design model of UVA-DIW printing of a urethane-CNT micro-coil and (right) micrograph of urethane micro-coil.<sup>[41]</sup> Copyright 2014 Royal Society of Chemistry.

they possess compliant properties as found in tissue and good biocompatibility.<sup>[45]</sup> The UVA-DIW methods are primarily used to print biocompatible lattice structured scaffold for drug delivery, bio-integrative tissue lattices, and microfluidics.<sup>[46, 47]</sup> A UVA-DIW ink using photocurable PDMS manufactured lattice structures for bio-integrative cellular structures and microfluidic tubing.<sup>[46]</sup> This formulation consisted of a (methacryloxypropyl)methylsiloxane–dimethylsiloxane copolymer, a commercially available methacrylated photosensitive siloxane, along with Sylgard 184 siloxane base and corresponding curing agent. The mixture used a dual-cure method for initial crosslinking of the photosensitive PDMS and a subsequent

thermal cure of the Sylgard 184 components (Fig. 6a). This photocurable PDMS ink was able to produce cellular geometries (Fig. 6b), which are a critical configuration for biocompatible structures. UVA-DIW using the same UV-curable PDMS also produced hollow tube extrusions (Fig. 6c) for microfluidic applications.<sup>[46]</sup>

UVA-DIW enabled another photosensitive PDMS elastomeric lattice material to be used as drug delivery devices by incorporating a stand-in drug dosage of Prednisone into the ink.<sup>[47]</sup> The drug delivery systems were demonstrated using a commercial bioprinter, Bio Bots 1 (Fig. 6d), to deposit lattices with the large surface area for engineered delivery of the

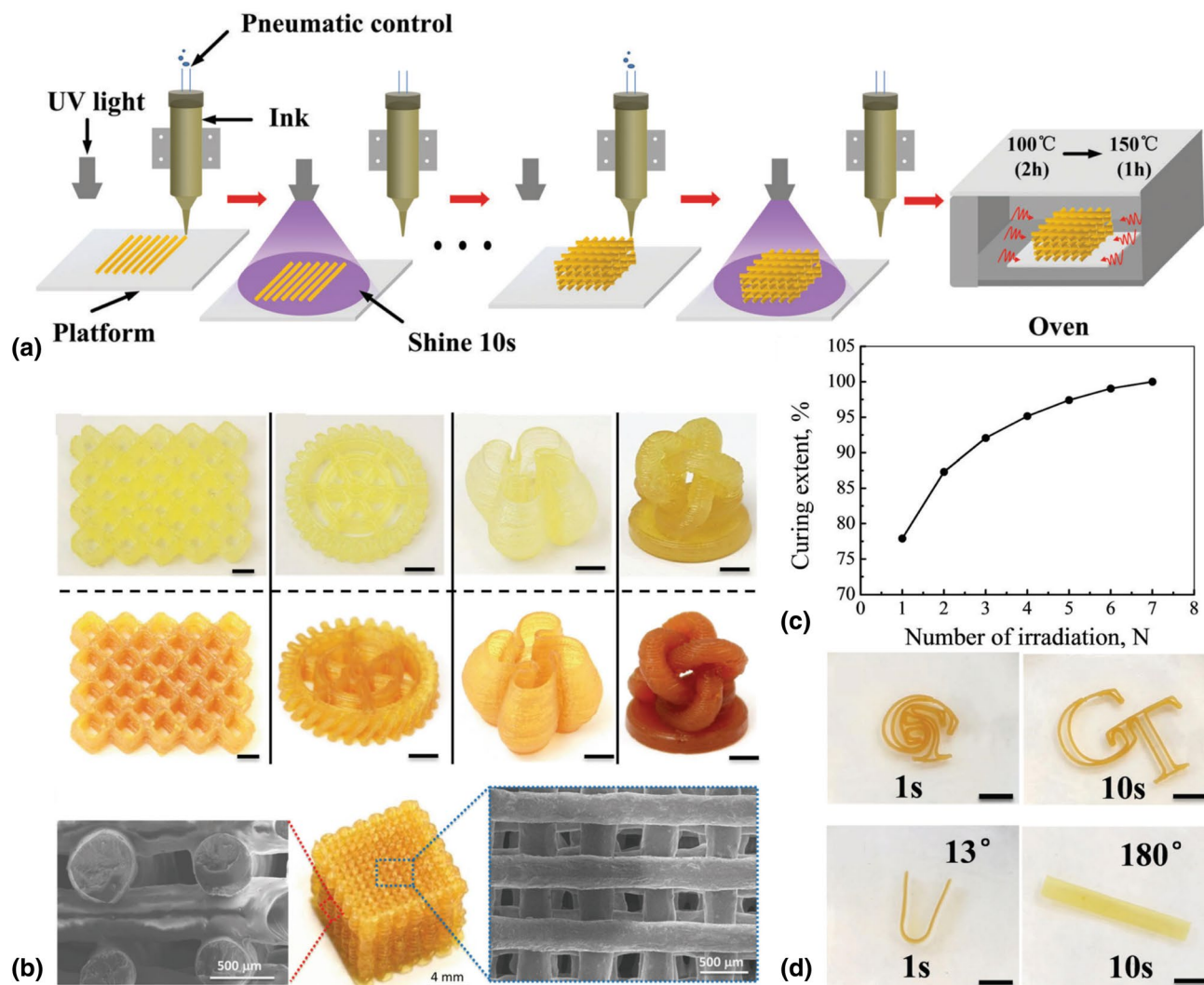


**Figure 5.** Dual-cure epoxy UVA-DIW systems. (a) Shape memory epoxy nanocomposites manufacturing process. (b) Complex epoxy-silica-printed structures with scale bars representing 4 mm. (c) Curing extent in relation to the 10s irradiation exposure steps. (d) Shape memory recovery of dual-cure epoxy with scale bars representing 4 mm.<sup>[44]</sup> Copyright 2018 Royal Society of Chemistry.

Prednisone. The tailored surface area determined by the lattice spacing and diameter is useful for engineering drug dosage amounts. The best printing quality was shown at a drug loading of 1.5% in the PDMS solution (Fig. 6e), but with the addition of viscosity modifying liquids, a drug loading of up to 10% was possible. These compliant and biocompatible PDMS structures produced by UVA-DIW provide the ability to tailor lattice infill for surface area and drug loading to optimize for a specified rate of drug dispersion.

UVA-DIW has also been successful in manufacturing bio-integrative and stimuli-responsive hydrogel structures. Hydrogels are polymer networks swollen by water with intrinsic mechanical flexibility, low density, hydrophilicity, and other properties similar to natural biological materials.<sup>[48]</sup> Photocrosslinkable hydrogels are commonly polymerized by a free-radical chain- or step-growth crosslinking. DIW has a unique

advantage in printing hydrogels because of the ability to tailor their viscoelastic properties by altering the solvent-to-monomer ratio. Uchida et al. used freeform reversible embedding (FRE) printing for hydrogel printing, where FRE is a novel form of bio-centric DIW that utilizes a suspension medium to retain deposition locations.<sup>[49, 50, 59]</sup> The FRE method allows for multidimensional control over deposition locations, and when adapted to the UVA-DIW process, UV light is transmitted through suspension medium and photopolymerizes the printed filament. The viscous suspension gel in an open vat was used as a receptacle for the deposition of hydrogel inks in a freeform 3D space to produce stimuli-responsive hydrogels. The deposition of the hydrogel into the suspension is governed by several flow parameters that comprise an appropriate extrusion rate (Fig. 7a). The flow parameters set within the study include  $v$  stage speed,  $Q$  volumetric flow rate,  $h$  height of nozzle in vat,



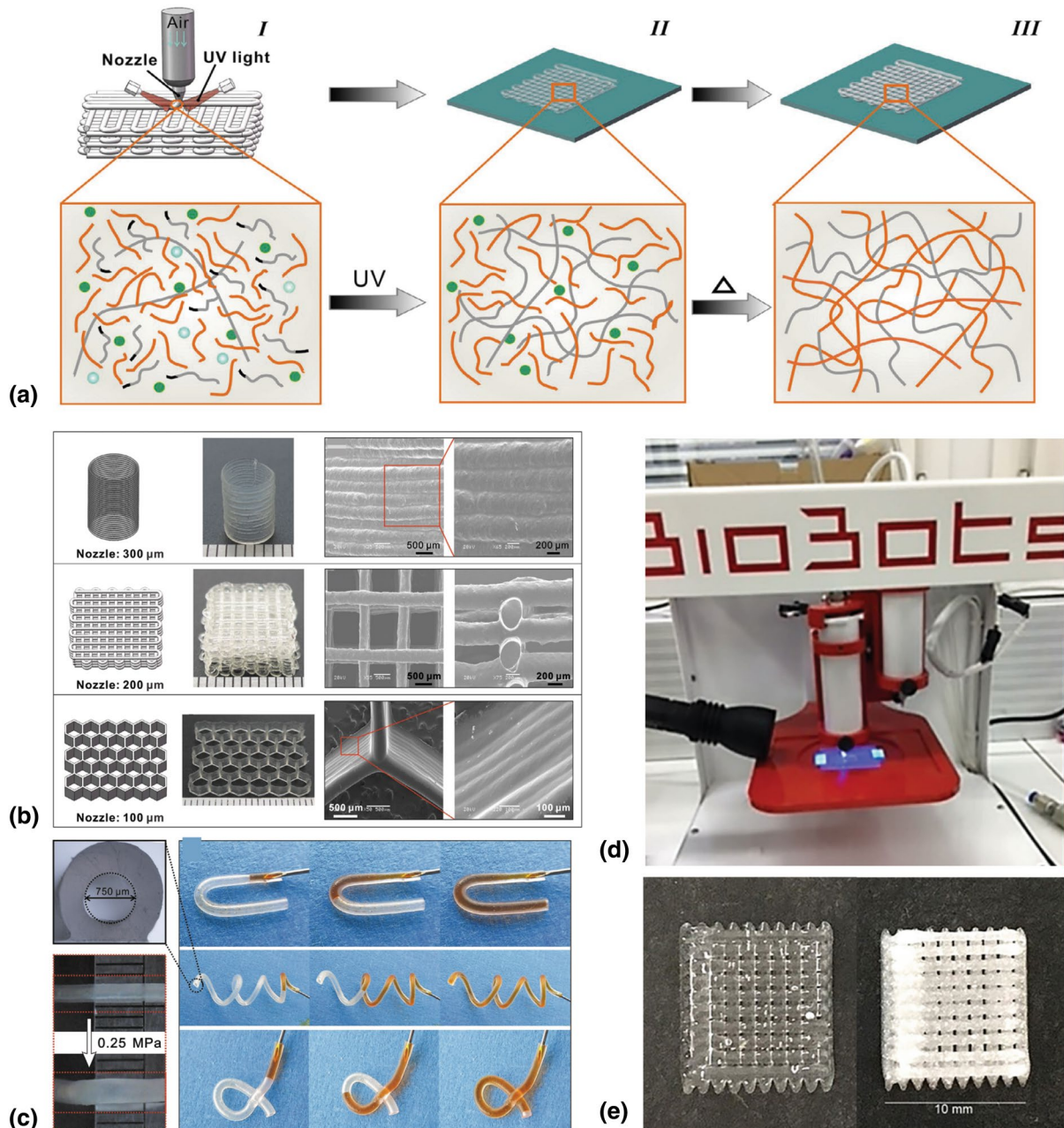


**Figure 6.** UVA-DIW of siloxanes. (a) (I) Printable ink chemistry with unreacted methacrylated PDMS (gray line), Sylgard 184 precursor (orange line), UV initiator (blue dots), and thermal initiator (green dots). (II) UV polymerization of the methacrylated PDMS and (III) final thermal curing of the Sylgard 184 PDMS. (b) Multilayer UVA-DIW-extruded architectures and cellular structures. (c) PDMS-printed hollow shells and their microfluidic capabilities.<sup>[46]</sup> Copyright 2018 Elsevier. (d) Bio Bots 1 Bioprinter commercial machine with UVA-DIW modifications and (e) (left) PDMS-Prednisone drug delivery lattice with 0% weight percent Prednisone and (right) 1.5% weight percent Prednisone.<sup>[47]</sup> Copyright 2017 Elsevier.

$C_{\text{NaA}}(\text{w/w})\%$  sodium alginate in the ink, and  $C_{\text{CMC}}(\text{w/w})\%$  carboxymethyl cellulose (CMC) of the suspension, which are used to accurately deposit a uniform stream of hydrogel at a specified Z-height in the suspension. Optimizing these flow parameters results in a constant uniform stream of filament at approximately the same inner diameter size of the deposition nozzle. Once their hydrogel material  $C_{\text{NaA}}(\text{w/w})\%$ , suspension

medium  $C_{\text{CMC}}(\text{w/w})\%$ , and flow rate parameters were optimized for printing, a fully freeform structure was then irradiated and removed from the suspension (Fig. 7b).

One issue encountered in vat printing hydrogels using the UVA-DIW process is the infiltration of the vat medium into the printed hydrogel filament.<sup>[50]</sup> The infiltration is governed by the affinity between the hydrogel ink and the suspension





the surrounding printed material. An issue in this process is that consecutive layers may decrease in viscosity due to the higher temperature, thus decreasing structural stability as the printed structure increases in size. However, these concerns are mitigated with precisely engineered deposition rates and knowledge of the reaction rate. Several of the fundamental studies on RAM used two-part monomers stored in separate reservoirs and deposited through a tortuous-path-mixing nozzle (Fig. 8a).<sup>[51–53]</sup>

Rios et al. used a reactive polymer from PPG Industries, Inc. to investigate the transient cure properties for the reactive polymers.<sup>[51]</sup> The study investigated the curing of the reactive polymer system from 0 to 120 s after being mixed. They showed the transient non-linear rate of polymerization within the selected material based on absorbance (Fig. 8b). In addition to the absorbance, the more structural metric for the reactive polymer is measured by observing the storage modulus increase, which also correlates to the yield strength increase within the material (Fig. 8c). This RAM process produces parts that exhibit a strain-to-failure ratio of 61% using a reactive polymer blend compared to a lower strain-to-failure ratio of

3% for FFF-printed Nylon and 5% for FFF-printed ABS, demonstrating the favorable interlayer strength due to the reactive crosslinking. Due to RAM's ambient temperature extrusion and low thermal expansion, RAM can be readily applied to large-scale additive manufacturing.

Large-scale RAM is another reactive cure DIW method that has been shown to print at high volumetric rates (~7 kg/h) of rapidly curing thermoset materials (Fig. 8d).<sup>[53, 54]</sup> The large-scale RAM systems possess low thermal expansion because ambient extrusion prevents large heat differentials between deposited material layers, overcoming some residual thermal stress issues which thermoplastic big area additive manufacturing has encountered.<sup>[5, 55]</sup> Ambient extrusion and subsequent crosslinking between partially cured layers exhibit improved build quality through lower temperature gradients and crosslinked interlayer properties.<sup>[56]</sup> The increase of yield strength from the reactive curing enables the proceeding layers to withstand their own weight better, allowing for the printing of larger structures. Hershey et al. used large-scale RAM to create sparse infill patterns that are vital to reducing weight in additively produced parts and demonstrating the integrity of

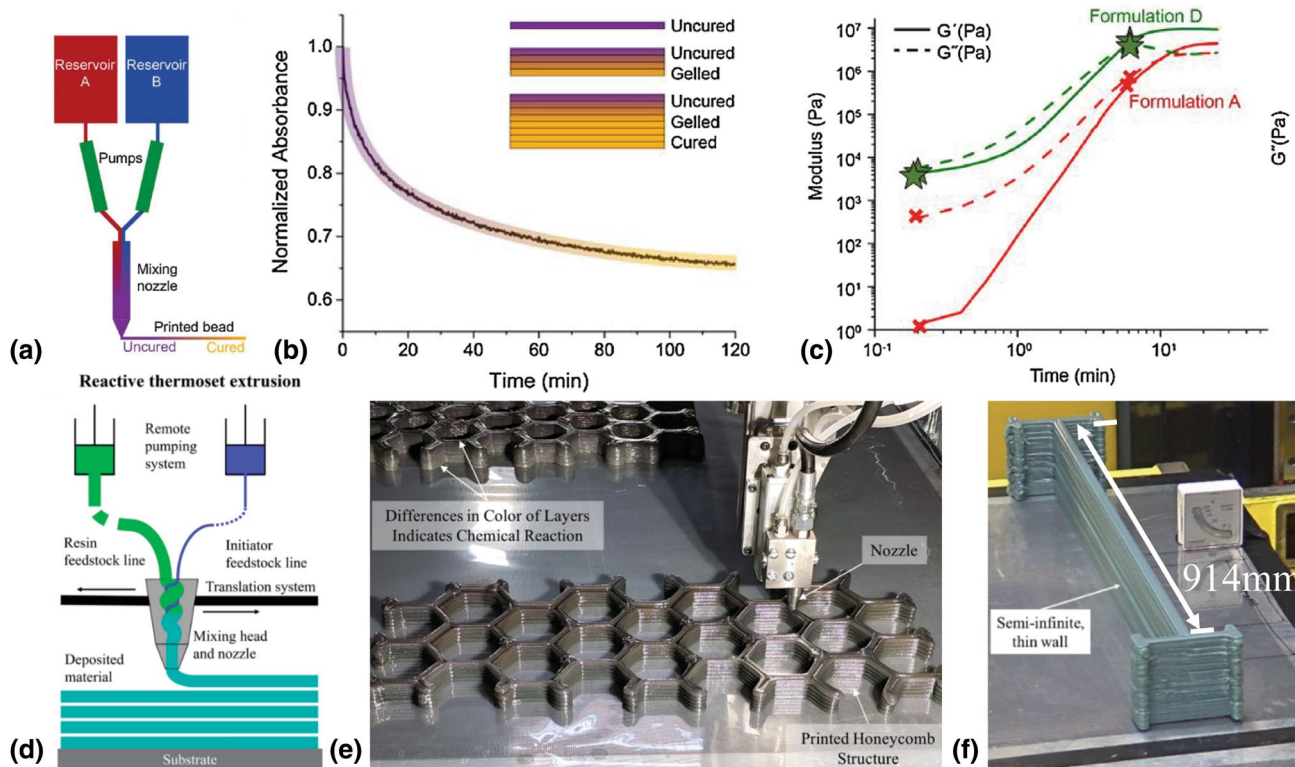


**Figure 8.** Large-scale RAM-based manufacturing schemes. (a) RAM printing method using mixing of monomer and initiator from two reservoirs and transition from uncured to cured material after deposition. (b) Normalized absorbance of curing of a reactive polymer system over time. (c) Storage and loss modulus development of Formulation A and D, which are two candidate rapid curing thermoset systems investigated with RAM. The set of stars and green lines represent successful printing, and the 'x's and red lines represent unsuccessful printing times during the reactive cure. The stars and 'x's after being mixed at 0.2 min, and after a period of cure, 7 min, show the rapid increase in moduli upon mixing of the reactive inks.<sup>[51]</sup> Copyright 2018 Elsevier. (d) Large-scale RAM system mixing monomer and initiator for in situ curing.<sup>[56]</sup> (e) Large-scale RAM cellular structure showing the gradient in curing rate by layer color.<sup>[53]</sup> (f) Large-scale RAM thin wall sample printed at a length of 914 mm.<sup>[56]</sup> Reprinted by permission from the Society for the Advancement of Material and Process Engineering (SAMPE).

the printed filament undergoing exothermic reaction.<sup>[57]</sup> The curing process can be observed by the change in layer colors, for example, dark (cured) to light (uncured), as the material is being printed (Fig. 8e). The rate of color change guides appropriate print speeds to retain structural support printing. Conventionally processed thermoset components of this size would be challenging since they typically require thermal curing and would need a comparably sized oven to perform curing at elevated temperatures for uniform heating. Instead, using RAM significantly increases the rate of production of the large components by curing in situ. Full-size large-scale RAM samples are printed (Fig. 8f) without the thermal post-processing steps commonly needed for complete crosslinking in thermoset materials.

Poly(urethane) thermosets have been printed with a short working time (seconds to several minutes) using a viscous suspension material that retains the placement of the ink in a 3D matrix. This unique RAM technique was referred to as rapid liquid prototyping, RLP.<sup>[58]</sup> The polymer gel suspension used in this study is Carbomer 940, which is poly(acrylic acid) dissolved in water at 0.5% (w/v, i.e., g of solute/100 mL of solution). A neutralizing agent was added to maintain the pH at approximately 7.0 due to ideal gelation occurring at a pH range between 6.0 and 9.0. The suspension at 0.5% (w/v) was able to successfully suspend materials at significantly different density levels, as low as foam (0.27 g/cm<sup>3</sup>) and up to steel (7.75 g/cm<sup>3</sup>). The Carbomer 940 suspension gel allowed printing with the suppressed turbulent flow by high enough viscosity and shear-thinning properties when the dispensing nozzle tip shear through the medium. The suspension gel provides a medium for inks to be printed without requiring underlying support, and the suspension gel also remains thermally stable, dissipating heat generated in the exothermic reaction without lowering the gel's viscosity. The limited accuracy of the printed filaments in the medium and the reuse of the suspension gel are two key challenges with the RLP method. The RLP approach reports that the Carbopol 940 hydrogel can be used for up to 3 months (if the water evaporation from the vat is mitigated) and perform more than 20 individual printing sessions.

RAM is also explored using FRE for printing freeform structures out of biomaterials, further referred to as RAM-FRE. RAM-FRE is more prevalent in the bioengineering field for printing materials such as PDMS, collagen, and other hydrogels.<sup>[59]</sup> A study has been conducted on RAM-FRE-printed hydrophobic PDMS, which were printed within support vats consisting of hydrophilic poly(acrylic acid) granular gels. Once the PDMS ink is deposited in the suspension, the ink was then cured over 72 h at room temperature or 2 h at 65°C (Fig. 9a). Using this RAM-FRE method, freeform coils as well as other geometries were printed that exhibited superior inter-layer crosslinking (Fig. 9b). The RAM-FRE method of printing PDMS inks in a poly(acrylic acid) granular gel has shown that using a hydrophilic pre-gel suspension is promising for reducing infiltration and dilution of the hydrophobic prepolymer filament.

Lee et al. used the RAM-FRE processes to print and solidify acidified collagen.<sup>[60]</sup> The rapid solidification was accomplished via pH change to coagulate the collagen after being deposited in a pH-neutral suspension gel. The gelatin microparticle suspension in the RAM-FRE process neutralizes the acidic collagen, causing it to coagulate and solidify. The solidification occurs more precisely when the acidified collagen is printed at pH of 3.5 transitioning to pH of 7.4. Once the collagen coagulated, the suspension was heated above 37°C, which caused the suspension to lower in viscosity, allowing the collagen component to be removed from the suspension. The coagulated collagen structures are promising for bio-implants that allow for cellular encapsulation of living cells.

Hinton et al. explored a wider range of suspended hydrogel materials using in situ curing of alginate, collagen, and fibrin (Fig. 9c).<sup>[61]</sup> Their study used similar support and release mechanism to that of Lee et al., in which the printed hydrogel could be cured in situ and then released from the suspension matrix by increasing the temperature of the matrix to 37°C. The authors used 3D tomography and other imaging techniques to visualize and print objects at a 200 μm resolution. RAM-FRE printed various tissue-mimicking objects on branched coronary arteries, trabeculated embryonic hearts, and human brains. They aimed to use the geometric advantages of printing and solidification within a suspension to print proof of concept biological structures, replicating internal and external features. These biologically relevant architectures are promising for developing synthetic or bio-integrative designs using a single-print process implemented through the RAM-FRE method.

### SC-3D

SC-3D is another form of DIW, which utilizes rapid solvent evaporation as a solidification method for forming self-supporting structures.<sup>[62–65]</sup> SC-3D has been used to print micro-coils in complex sensor arrays, microfluidic channels, and lattice scaffolding. What governs the critical solidification for these applications are the solvent-to-solute concentration of the ink and how the solvents evaporate when exposed to atmospheric pressure. Conventional DIW solvent evaporation techniques use water as the evaporative solvent because of its polar properties, commonality, and non-toxicity. However, many ink formulations for SC-3D printing are made using higher vapor pressure solvents mixtures such as dichloromethane (DCM) that evaporate rapidly to induce solidification shortly after being extruded. This phenomenon is referred to as flash vaporization, where the solvent evaporates when exposed to a much lower ambient atmospheric pressure [Fig. 10a (right)]. The solvent evaporation of the deposited filaments results in a rapid increase in viscosity and yield strength to the point of self-support during printing. The solvent content decreases after being exposed to the ambient atmosphere (Fig. 10a (bottom-left)) and continues to decrease for multiple hours after deposition. The ink is also engineered with a shear-thinning behavior determined by solute loading, which aids at some degree with



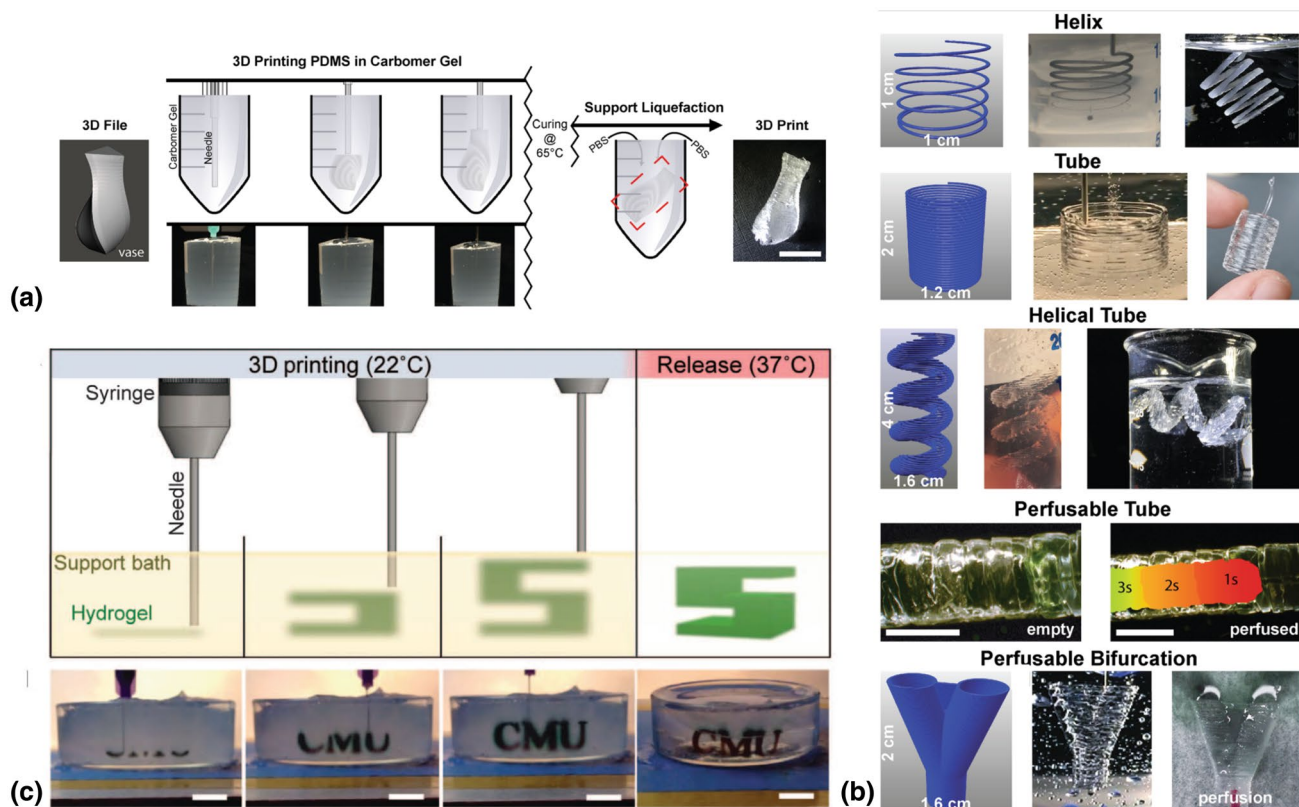


**Figure 9.** RAM-FRE methods printing fast solidification inks within a suspension gel. (a) RAM-FRE process for printing PDMS inks in poly(acrylic acid)–water suspension gel with the temperature increase to remove the solidified PDMS structure. (b) (Top-to-bottom) RAM-FRE PDMS helical spiral, tube, helical tube, perfusable tube, and perfusable bifurcation.<sup>[59]</sup> Copyright 2016 American Chemical Society under CC BY license. (c) Printing sequence of hydrogel into support bath (top) graphical and (bottom) real deposition and release imagery.<sup>[61]</sup> Copyright 2015 Hinton et al. republished under the Creative Commons Attribution license.

passive self-support (Fig. 10a (top-left)). Solvent toxicity and volumetric shrinkage from solvent evaporation is one of the most significant challenges faced by SC-3D printing. DCM is a common solvent exhibited in SC-3D studies, however, it is toxic to humans as with several other toxic vapors found in solvent casting.<sup>[33, 66]</sup> Studies have also been conducted to appropriately formulate solutions based on a range of differing vapor pressure solvents as well as dissolved polymer filler to confront the mass loss during printing.<sup>[62, 65]</sup>

A study for the flash vaporization of SC-3D extrusion investigated and characterized freeform helical spirals that function as strain sensors.<sup>[62]</sup> In this study, a highly concentrated poly(lactic acid) (PLA) solution dissolved in DCM was used for forming microscale helical spirals. It was found that the diameter of the nozzles (200  $\mu\text{m}$ , 330  $\mu\text{m}$ , and 510  $\mu\text{m}$ ) impacted the printing quality, where smaller nozzles allowed for better freeform printability (Fig. 10a). The solidification was the fastest with the 200  $\mu\text{m}$  nozzle because the entrapped solvent within the filament requires a shorter distance to reach the atmosphere. Higher concentration of PLA allowed for a lower percentage of shrinkage and inherently more viscous solution, providing self-supporting properties. The self-supporting capabilities draw

from the relationship of the diameter of the nozzle, which is proportional to the solvent evacuation rate from the filament, and the PLA solute content with its initial viscosity contribution (Fig. 10b).

Wu et al. successfully printed micro-coils by SC-3D.<sup>[64]</sup> Using a solution consisting of 30 wt% PLA and 70 wt% DCM, this study printed multilayer 2D lattices and completely freeform print paths (Fig. 10c). The geometries in the study were directed toward high-precision engineering applications, specifically for freeform microfluidic channels (Fig. 10d), showing promise in biomedical applications for microvasculature and drug delivery. In addition, a similar solid micro-coil was coated in copper to perform as a radio-frequency antenna, which exhibited potential applications of SC-3D in flexible electronics (Fig. 10e).

The solvent evaporation relationship to the volumetric shrinkage of chitosan laden inks by SC-3D printing has also been investigated (Fig. 10f).<sup>[65]</sup> The study formulated two inks with 8 wt% of chitosan, one using an acetic acid mixture (40 vol% acetic acid) and the other using an acetic–lactic–citric acid mixture (40 vol% acetic acid, 20 vol% lactic acid, and 3 wt% citric acid). The SC-3D printing with the acetic acid

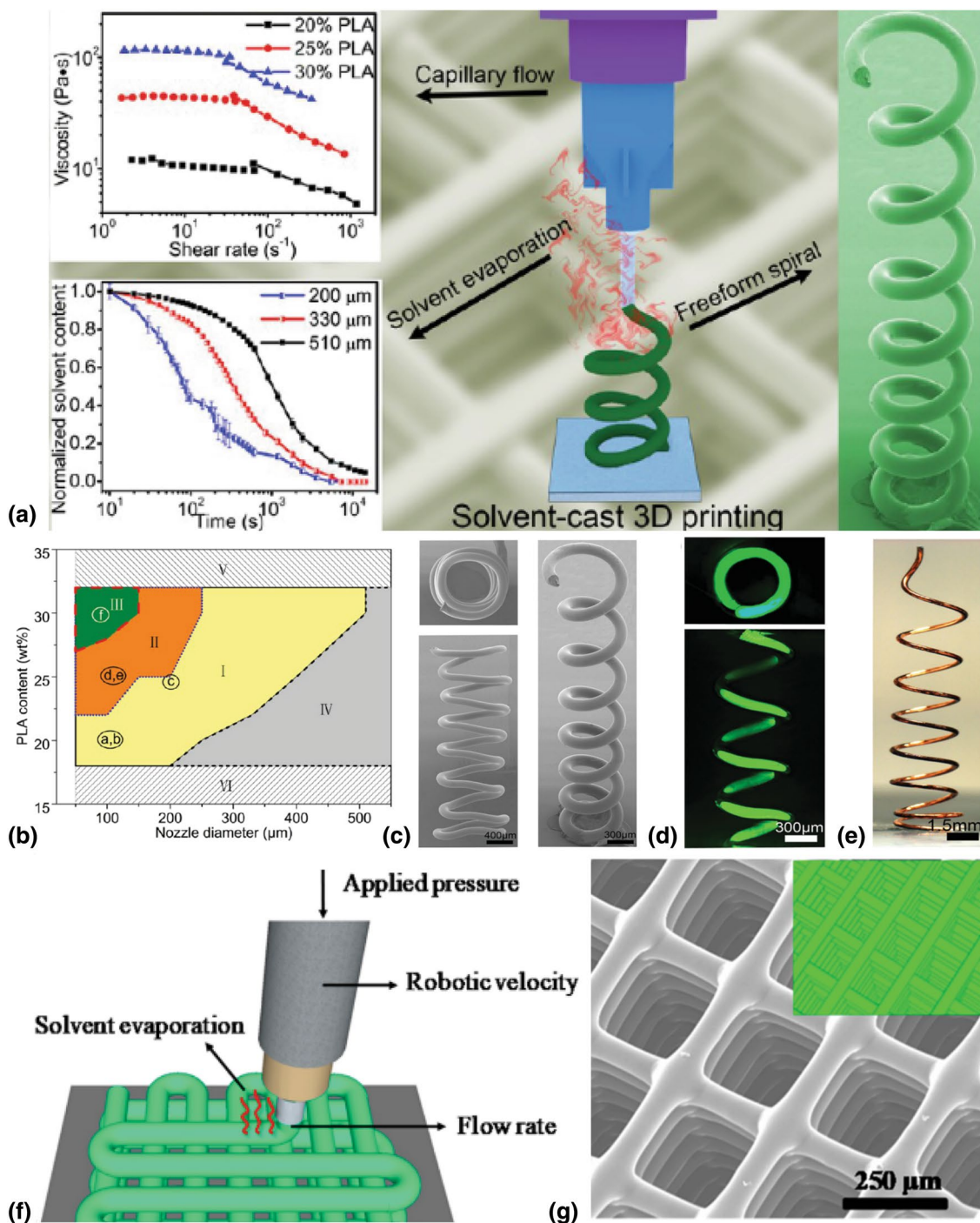


**Figure 10.** SC-3D printing of lattices and freeform spirals. (a) (Top-left) viscosity to shear rate relationship with respect to PLA solute content, (bottom-left) normalized solvent content to time relationship for different nozzle sizes and (right) the solvent cast printing poly(acrylic acid) solution with flash evaporation. (b) Printability map relating solute content to nozzle diameter where (I) 1D filaments, (II) 2D lattice layer stacking, (III) fully freeform printability, and (IV) unviable.<sup>[62]</sup> Copyright 2014 American Chemical Society. (c) SEM image of a freeform SC-3D coil. (d) Fluorescent microscopy of fluid in hollow micro-coil. (e) Copper-coated micro-coil antenna.<sup>[64]</sup> Copyright 2013 John Wiley and Sons. (f) Printing of 2D lattices using chitosan laden ink. (g) SEM image of periodic 2D chitosan laden lattices and (top-right inset) their corresponding digital pathing model.<sup>[65]</sup> Copyright 2018 American Chemical Society.

mixture solely contained the higher vapor pressure solvent acetic acid, which provided flash vaporization but resulted in too much shrinkage. Thus, the study prioritized the acetic–lactic–citric mixture for printing because it persevered geometric dimensionality best after flash vaporization behavior. The printing from the acetic–lactic–citric acid mixture indicated that optimal SC-3D inks are composed of high vapor pressure solvents as well as other more slowly evaporative solvents that retain the shape and mass of the uncured structure until a post-process step for full solidification. The printed chitosan lattices retain their intended shape, determined by a digitized model, after full solidification (Fig. 10g). This shape retention is important for having viable uniform structures when fully processed, which avoids cracks or internal stresses from SC-3D flash vaporization solidification.

## Conclusion and perspectives

In situ solidification in DIW has shown to be a promising avenue for improving geometric resolution, freeform fabrication, build heights, and overhang angles. The 3D structures in multiple applications are manufactured through three primary in situ curing methods discussed in this review: UVA-DIW, RAM, and SC-3D:

- (1) UVA-DIW technologies have been shown to enhance the resolution of additively manufactured high-performance polymers such as polyimides and epoxies by improving shrinkage resistance and resolution in dual-cure systems. UVA-DIW has also shown structural enhancements for forming elastomeric networks of crosslinked acrylates for shape memory materials. The acrylate crosslinking has also helped to achieve fully self-supporting photocurable urethane and epoxy nanocomposites as well as hydrogels within a suspension medium.
- (2) RAM has shown to be promising for large-scale additive manufacturing for thermosets due to the elimination of the post-curing step by the in situ curing. Large-scale RAM printing allows for large volumes of material to be deposited while retaining geometry and providing improved interlayer strength. Components printed using RAM were also demonstrated as viable biocompatible structures using PDMS, collagen, and hydrogel inks printed into a viscous suspension gel.
- (3) SC-3D printing has demonstrated enhancements in dimensionality retention by using high solute loading and flash vaporization to incur self-supporting yield strength. These SC-3D methods have provided low-cost avenues for accurately manufacturing mechanical and electrical microsystems, and have also shown manufacturability of biomaterials.

Each of the DIW in situ curing methods has unique manufacturability that allowed for vital free-standing and

self-supporting components for high-performance polymer systems. In addition, the intricate geometrical rendering, versatile materials selection, and post-modification offered by DIW in situ curing enable applications ranging from microelectronics, soft robotics to biomedical therapeutics. Finally, considering the resemblance of the DIW in situ curing to nature's bottom-up material forming capability optimized with minimized energy and resource consumption, DIW in situ curing may provide sustainable, cost-efficient processing approaches to manufacture high-value complex objects.

## Acknowledgments

This research was sponsored by the Laboratory Directed Research and Development Program of Oak Ridge National Laboratory, managed by UT-Battelle, LLC, for the U.S. Department of Energy. JKW would like to acknowledge support from the U.S. Department of Energy, Office of Science, Office of Workforce Development for Teachers and Scientists (WDTS) under the Science Undergraduate Laboratory Internship program. BGC would like to acknowledge support from Honeywell Federal Manufacturing and Technologies through contract DE-NA0002839.

## Compliance with ethical standards

### Conflict of interest

No conflicts to declare.

### Ethical approval

This article does not contain any studies with human participants or animals performed by any of the authors.

## References

1. T.D. Ngo, A. Kashani, G. Imbalzano, K.T.Q. Nguyen, D. Hui, Additive manufacturing (3D printing): a review of materials, methods, applications and challenges. *Composites B* **143**(2017), 172–196 (2018)
2. H. Quan, T. Zhang, H. Xu, S. Luo, J. Nie, X. Zhu, Bioactive materials photocuring 3D printing technique and its challenges. *Bioact. Mater.* **5**(1), 110–115 (2020)
3. G. Ding, R. He, K. Zhang, M. Xia, C. Feng, D. Fang, Dispersion and stability of SiC ceramic slurry for stereolithography. *Ceram. Int.* **46**(4), 4720–4729 (2020)
4. R. He, G. Ding, K. Zhang, Y. Li, D. Fang, Fabrication of SiC ceramic architectures using stereolithography combined with precursor infiltration and pyrolysis. *Ceram. Int.* **45**(11), 14006–14014 (2019)
5. B.N. Turner, S.A. Gold, A review of melt extrusion additive manufacturing processes: II. Materials, dimensional accuracy, and surface roughness. *Rapid Prototyp. J.* **21**(3), 250–261 (2015)
6. N.S. Hmeidat, R.C. Pack, S.J. Talley, R.B. Moore, B.G. Compton, Mechanical anisotropy in polymer composites produced by material extrusion additive manufacturing. *Addit. Manuf.* **34**, 101385 (2020)
7. R.L. Truby, J.A. Lewis, Printing soft matter in three dimensions. *Nature* **540**(7633), 371–378 (2016)



8. L. Li, Q. Lin, M. Tang, A.J.E. Duncan, C. Ke, Advanced polymer designs for direct-ink-write 3D printing. *Chem. Eur. J.* **25**(46), 10768–10781 (2019)
9. S. Roh, D.P. Parekh, B. Bharti, S.D. Stoyanov, O.D. Velev, 3D printing by multiphase silicone/water capillary inks. *Adv. Mater.* **29**, 1–7 (2017)
10. N.S. Hmeidat, J.W. Kemp, B.G. Compton, High-strength epoxy nanocomposites for 3D printing. *Compos. Sci. Technol.* **160**, 9–20 (2018)
11. P. Jiang, C. Yan, Y. Guo, X. Zhang, M. Cai, X. Jia, X. Wang, F. Zhou, Direct ink writing with high-strength and swelling-resistant biocompatible physically crosslinked hydrogels. *Biomater. Sci.* **7**, 1805–1814 (2019)
12. H. Chen, X. Wang, F. Xue, Y. Huang, K. Zhou, D. Zhang, 3D printing of SiC ceramic : direct ink writing with a solution of preceramic polymers. *J. Eur. Ceram. Soc.* **38**(16), 5294–5300 (2018)
13. J.W. Kemp, N.S. Hmeidat, B.G. Compton, Boron nitride-reinforced polysilazane-derived ceramic composites via direct-ink writing. *J. Am. Ceram. Soc.* **103**(8), 4043–4050 (2020)
14. B. Chen, Y. Jiang, X. Tang, Y. Pan, S. Hu, Fully packaged carbon nanotube supercapacitors by direct ink writing on flexible substrates. *Appl. Mater. Interfaces* **9**, 28433–28440 (2017)
15. J.P. Lewicki, J.N. Rodriguez, C. Zhu, M.A. Worsley, A.S. Wu, Y. Kanarska, J.D. Horn, E.B. Duoss, J.M. Ortega, W. Elmer, R. Hensleigh, R.A. Fellini, M.J. King, 3D-printing of meso-structurally ordered carbon fiber/polymer composites with unprecedented orthotropic physical properties. *Sci. Rep.* **7**(43401), 1–14 (2017)
16. Y. Jiang, Z. Xu, T. Huang, Y. Liu, F. Guo, J. Xi, W. Gao, Direct 3D printing of ultralight graphene oxide aerogel microlattices. *Adv. Funct. Mater.* **1707024**, 1–8 (2018)
17. T.V. Neumann, E.G. Facchine, M.D. Dickey, B. Leonardo, S. Khan, Direct write printing of a self-encapsulating liquid metal–silicone composite. *Soft Matter* **16**, 6608–6618 (2020)
18. L. Wei, J. Li, S. Zhang, B. Li, Y. Liu, F. Wang, S. Dong, Fabrication of SiOC ceramic with cellular structure via UV-assisted direct ink writing. *Ceram. Int.* **46**, 3637–3643 (2020)
19. J.A. Lewis, Direct-write assembly of ceramics from colloidal inks. *Curr. Opin. Solid State Mater. Sci.* **6**, 245–250 (2002)
20. F. Peng, B.D. Vogt, M. Cakmak, Complex flow and temperature history during melt extrusion in material extrusion additive manufacturing. *Addit. Manuf.* **22**, 197–206 (2018)
21. S.K. Romberg, M. Islam, C.J. Hershey, M. Devinney, C.E. Duty, V. Kunc, B.G. Compton, Linking thermoset ink rheology to the stability of 3D-printed structures. *Addit. Manuf.* (2020). <https://doi.org/10.1016/j.addma.2020.101621>
22. H. Bikas, P. Stavropoulos, G. Chryssolouris, Additive manufacturing methods and modelling approaches : a critica review. *Int. J. Adv. Manuf. Technol.* **83**, 389–405 (2015)
23. L.C. Sanchez, C. Augusto, G. Beatrice, S. Helena, P. Bettini, L.C. Costa, Rheological approach for an additive manufacturing printer based on material extrusion. *Int. J. Adv. Manuf. Technol.* **105**, 2403–2414 (2019)
24. N. Kretzschmar, S. Lipponen, V. Klar, J.M. Pearce, T.L. Ranger, Mechanical properties of ultraviolet-assisted paste extrusion and postextrusion ultraviolet-curing of three-dimensional printed biocomposites. *3D Print. Addit. Manuf.* **6**(3), 127–137 (2019)
25. A. M'Barki, L. Bocquet, A. Stevenson, Linking rheology and printability for dense and strong ceramics by direct ink writing. *Sci. Rep.* **7**(1), 1–10 (2017)
26. C. Duty, C. Ajinjeru, V. Kishore, B. Compton, N. Hmeidat, X. Chen, P. Liu, A. Arabi, J. Lindahl, V. Kunc, What makes a material printable ? A viscoelastic model for extrusion-based 3D printing of polymers. *J. Manuf. Process.* **35**(September), 526–537 (2018)
27. B. Narupai, A. Nelson, 100th Anniversary of macromolecular science viewpoint: macromolecular materials for additive manufacturing. *ACS Macro Lett.* **9**, 627–638 (2020)
28. V.C.F. Li, C.K. Dunn, Z. Zhang, Y. Deng, H.J. Qi, Direct ink write (DIW) 3D printed cellulose nanocrystal aerogel structures. *Sci. Rep.* **7**(1), 1–8 (2017)
29. J.A. Lewis, Direct ink writing of 3D functional materials. *Adv. Funct. Mater.* **16**(17), 2193–2204 (2006)
30. J.A. Lewis, Colloidal processing of ceramics. *J. Am. Ceram. Soc.* **83**(10), 2341–2359 (2000)
31. A.C. De Leon, Q. Chen, N.B. Palaganas, J.O. Palaganas, J. Manapat, R.C. Advincula, High performance polymer nanocomposites for additive manufacturing applications. *React. Funct. Polym.* **103**, 141–155 (2016)
32. J.E. Smay, J. Cesarano, J.A. Lewis, Colloidal inks for directed assembly of 3-D periodic structures. *Langmuir* **18**(14), 5429–5437 (2002)
33. E. Peng, D. Zhang, J. Ding, Ceramic robocasting: recent achievements, potential, and future developments. *Adv. Mater.* **30**(47), 1–14 (2018)
34. Z. Ji, X. Zhang, C. Yan, X. Jia, Y. Xia, X. Wang, F. Zhou, 3D printing of photocuring elastomers with excellent mechanical strength and resilience. *Macromol. Rapid Commun.* **40**(8), 1–6 (2019)
35. J.Z. Manapat, Q. Chen, P. Ye, R.C. Advincula, 3D printing of polymer nanocomposites via stereolithography. *Macromol. Mater. Eng.* **302**(9), 1–13 (2017)
36. H. Lipson, M. Kurman, *Fabricated the New World of 3D Printing* (Wiley, Hoboken, 2013).
37. D.A. Rau, J. Herzberger, T.E. Long, C.B. Williams, Ultraviolet-assisted direct ink write to additively manufacture all-aromatic polyimides. *ACS Appl. Mater. Interfaces* **10**(41), 34828–34833 (2018)
38. Y. Guo, J. Xu, C. Yan, Y. Chen, X. Zhang, X. Jia, Y. Liu, X. Wang, F. Zhou, Direct ink writing of high performance architected polyimides with low dimensional shrinkage. *Adv. Eng. Mater.* **21**(5), 1–8 (2019)
39. T. Wu, P. Jiang, X. Zhang, Y. Guo, Z. Ji, X. Jia, X. Wang, F. Zhou, W. Liu, Additively manufacturing high-performance bismaleimide architectures with ultraviolet-assisted direct ink writing. *Mater. Des.* **180**, 107947 (2019)
40. X. Kuang, K. Chen, C.K. Dunn, J. Wu, V.C.F. Li, H.J. Qi, 3D printing of highly stretchable, shape-memory, and self-healing elastomer toward novel 4D printing. *ACS Appl. Mater. Interfaces* **10**(8), 7381–7388 (2018)
41. R.D. Farahani, K. Chizari, D. Therriault, Three-dimensional printing of free-form helical microstructures: a review. *Nanoscale* **6**(18), 10470–10485 (2014)
42. L.L. Lebel, B. Aissa, M.A. El Khakani, D. Therriault, Ultraviolet-assisted direct-write fabrication of carbon nanotube/polymer nanocomposite microcoils. *Adv. Mater.* **22**(5), 592–596 (2010)
43. R.D. Farahani, L.L. Lebel, D. Therriault, Processing parameters investigation for the fabrication of self-supported and freeform polymeric microstructures using ultraviolet-assisted three-dimensional printing. *J. Micromech. Microeng.* **24**(5), 055020 (2014)
44. K. Chen, X. Kuang, V. Li, G. Kang, H.J. Qi, Fabrication of tough epoxy with shape memory effects by UV-assisted direct-ink write printing. *Soft Matter* **14**(10), 1879–1886 (2018)
45. S. Li, F.P.U. Severino, J. Ban, L. Wang, G. Pinato, V. Torre, Y. Chen, Improved neuron culture using scaffolds made of three-dimensional PDMS microlattices. *Biomed. Mater.* **13**(3), 034105 (2018)
46. Z. Ji, D. Jiang, X. Zhang, Y. Guo, X. Wang, Facile photo and thermal two-stage curing for high-performance 3D printing of poly (dimethylsiloxane). *Macromol. Rapid Commun.* **41**(2000064), 1–8 (2020)
47. J. Holländer, R. Hakala, J. Suominen, N. Moritz, J. Yliruusi, 3D printed UV light cured polydimethylsiloxane devices for drug delivery. *Int. J. Pharm.* **544**(2), 433–442 (2018)
48. E. Caló, V.V. Khutoryanskiy, Biomedical applications of hydrogels: a review of patents and commercial products. *Eur. Polym. J.* **65**, 252–267 (2015)
49. O. Jeon, Y.B. Lee, T.J. Hinton, A.W. Feinberg, E. Alsborg, Cryopreserved cell-laden alginate microgel bioink for 3D bioprinting of living tissues. *Mater. Today Chem.* **12**, 61–70 (2019)
50. T. Uchida, H. Onoe, 4D printing of multi-hydrogels using direct ink writing in a supporting viscous liquid. *Micromachines* **10**(7), 433 (2019)
51. O. Rios, W. Carter, B. Post, P. Lloyd, D. Fenn, C. Kutchko, R. Rock, K. Olson, B. Compton, 3D printing via ambient reactive extrusion. *Mater. Today Commun.* **15**(June 2017), 333–336 (2018)
52. J. Lindahl, A.A. Hassen, S. Romberg, B. Hedger, P.H. Peter Hedger, M. Walch, T. Deluca, W. Morrison, S. Kim, A. Roschli, D. Nuttal, J. Czachowski, B. Post, L. Love, V. Kunc, Large-scale additive manufacturing with reactive polymers, in *CAMX 2018-Composites and Advanced Materials Expo* (2018)
53. V. Kunc, J. Lindahl, A. Lee, M. Mathews, B. Post, L. Love, P. Liu, V. Kishore, S. Voeks, A.A. Hassen, Low cost reactive polymers for large scale additive manufacturing, in *CAMX 2018-Composites and Advanced Materials Expo* (2018)

54. V. Kunc, J. Ilkka, S. Voeks, J. Lindahl, *Vinylester and Polyester 3D Printing* (USDOE Office of Energy Efficiency and Renewable Energy (EERE), Advanced Manufacturing Office, 2018)
55. C.E. Duty, V. Kunc, B. Compton, B. Post, D. Erdman, R. Smith, R. Lind, P. Lloyd, L. Love, Structure and mechanical behavior of big area additive manufacturing (BAAM) materials. *Rapid Prototyp. J.* **23**(1), 181–189 (2017)
56. S.K. Romberg, C.J. Hershey, J.M. Lindahl, W. Carter, B.G. Compton, V. Kunc, Large-scale additive manufacturing of highly exothermic reactive polymer systems, in *International SAMPE Technical Conference* (2019)
57. C.J. Hershey, J.M. Lindahl, S.K. Romberg, A.C. Roschli, B. Hedger, M. Kastura, B.G. Compton, V. Kunc, Large-scale reactive extrusion deposition of sparse infill structures with solid perimeters, in *CAMX 2019—Composites and Advanced Materials Expo*, pp. 0–6 (2019)
58. K. Hajash, B. Sparrman, C. Guberan, J. Laucks, S. Tibbits, Large-scale rapid liquid printing. *3D Print. Addit. Manuf.* **4**(3), 123–131 (2017)
59. T.J. Hinton, A. Hudson, K. Pusch, A. Lee, A.W. Feinberg, 3D printing PDMS elastomer in a hydrophilic support bath via freeform reversible embedding. *ACS Biomater. Sci. Eng.* **2**(10), 1781–1786 (2016)
60. A. Lee, A. Hudson, J. Shiwerski, J.W. Tashman, T.J. Hinton, S. Yerneni, J.M. Bliley, P.G. Campbell, A.W. Feinberg, 3D bioprinting of collagen to rebuild components of the human heart. *Science* **365**(6452), 482–487 (2019)
61. T.J. Hinton, Q. Jallerat, R.N. Palchesko, J.H. Park, M.S. Grodzicki, H.J. Shue, M.H. Ramadan, A.R. Hudson, A.W. Feinberg, Three-dimensional printing of complex biological structures by freeform reversible embedding of suspended hydrogels. *Sci. Adv.* **1**(9), e1500758 (2015)
62. S. Guo, M. Heuzey, D. Therriault, Properties of polylactide inks for solvent-cast printing of three-dimensional freeform microstructures. *Langmuir* **30**, 1142–1150 (2014)
63. Z. Gou, A.J. Mchugh, Two-dimensional modeling of dry spinning of polymer fibers. *J. Nonnewton Fluid. Mech.* **118**, 121–136 (2004)
64. S.Z. Guo, F. Gosselin, N. Guerin, A.M. Lanouette, M.C. Heuzey, D. Therriault, Solvent-cast three-dimensional printing of multifunctional microsystems. *Small* **24**, 4118–4122 (2013)
65. Q. Wu, D. Therriault, M. Heuzey, Processing and properties of chitosan inks for 3D printing of hydrogel microstructures. *ACS Biomater. Sci. Eng.* **4**, 2643–2652 (2018)
66. M.V. Evans, J.C. Caldwell, Evaluation of two different metabolic hypotheses for dichloromethane toxicity using physiologically based pharmacokinetic modeling for in vivo inhalation gas uptake data exposure in female B6C3F1 mice. *Toxicol. Appl. Pharmacol.* **244**(3), 280–290 (2010)